Dynamic modeling of contact-line deformation: Comparison with experiment

Stanimir Iliev and Nina Pesheva
Institute of Mechanics, Bulgarian Academy of Sciences, Academician G. Bonchev Street 4, 1113 Sofia, Bulgaria

Vadim S. Nikolayev
ESEME, Service des Basses Températures, INAC/CEA, Grenoble, France
and ESEME, PMMH-ESPCI-P6-P7, 10, rue Vauquelin, 75231 Paris Cedex 5, France
(Received 6 February 2008; revised manuscript received 16 June 2008; published 21 August 2008)

The quasistatic contact-line dissipation model is applied to the dynamics of relaxation of periodically perturbed contact lines in the Wilhelmy plate geometry where a solid plate is withdrawn vertically at constant velocity from a bath of liquid. The resulting motion of the three-dimensional liquid meniscus is solved rigorously by numerical simulation. A detailed comparison is performed with the recent experimental results of Delon *et al.* [J. Fluid Mech. **604**, 55 (2008)] and with their hydrodynamic approach. The described approach exhibits a better agreement with the experiments than the mentioned hydrodynamic approach. The influence of nonlinearity on the contact-line relaxation dynamics is analyzed. The deviation from the behavior predicted within the contact-line elasticity model is discussed.

DOI: 10.1103/PhysRevE.78.021605 PACS number(s): 68.03.Cd, 05.90.+m, 68.08.Bc

I. INTRODUCTION

Many industrial processes involve motion of the triple liquid-gas-solid contact line. It is especially important in microfluidic devices where the liquid volumes are very small. The ratio of the contact-line length to the characteristic size of the liquid is then relatively large and the contact-line phenomena have a strong impact on the fluid behavior. The solid surface in contact with the liquid is not ideal. In most practically important cases, its heterogeneity is important. It can lead in particular to a contact-line deformation. While the static contact-line deformation has been studied extensively, the dynamics of the deformed contact line is under active discussion. It is important to develop an adequate theoretical description that would permit modeling of the motion of the contact line of complicated, possibly irregular shapes where the liquid meniscus needs to be considered in three-dimensions (3D). This problem is especially challenging for the partial wetting regime, where the application of the conventional hydrodynamic description (i.e., the Navier-Stokes equations with the no-slip boundary condition at the solid surface) leads to infinite viscous dissipation appearing because of the moving contact line. In reality, the dissipation in the contact-line vicinity is very large but finite, and an alternative theoretical description needs to be sought. Several alternative approaches have been suggested in the literature [1–4]. Testing of these approaches against existing experimental data and determination of the range of validity of the adopted approximations is a necessary step.

The approach [2,3] that we will call hereafter the "hydrodynamic approach" (HA) seems to be the most advanced. It makes use of the Navier slip condition to solve the dissipation divergence issue and allows the viscous bending of the meniscus to be calculated in the lubrication approximation. In this approach the slip length serves as a control parameter that permits the contact-line relaxation dynamics to be adjusted [5]. An extension of the lubrication approach initially proposed by Boender *et al.* [6] and rediscovered recently [7] permits one on the one hand to reduce the problem dimensionality and on the other hand to treat uniformly the whole liquid meniscus without cutting it into "inner" and "outer" regions. The inner region is defined as the contact-line vicinity where high viscous shear stresses lead to meniscus bending; the outer region is the rest of the liquid domain where other (capillary, gravitational, etc.) forces are dominant and the viscous stresses are often negligible. However, the HA requires solution of nonlinear and singular nonstationary partial differential equations, which is a difficult task. For this reason the problem was solved in [2] rigorously only for a stationary meniscus with a straight contact line where the mathematical problem can be reduced to ordinary differential equations. To analyze the relaxation of a deformed contact line, a linearization has been performed which corresponds to the case of infinitesimally weak contact-line deformation.

Another difficulty of the HA appears when low-viscosity liquids like water, studied, e.g., in [8], need to be considered. Since the characteristic size of the inner region grows with the viscosity (it is proportional to the $1/3$ power of the capillary number [9] which is itself proportional to the viscosity), there is a strong scale separation between the inner and outer regions in this case. On the one hand, the spatial grid used in the numerical calculation needs to be dense enough to resolve the viscous bending in the inner region. On the other hand, the grid should be uniform enough throughout the whole domain to avoid numerical instabilities. The satisfaction of both these requirements leads to prohibitively large calculation times in the 3D case. Another approach thus needs to be sought for low-viscosity fluids.

Such an approach, which we call the "contact-line dissipation" approach (CLDA) has been suggested previously [10–12]. It is a generalization of the earlier approach [13]. It assumes that the inner region is so small that it can be "contracted" to zero, which is equivalent to the statement that the whole viscous dissipation in the liquid is localized *at* the contact line. The advantage of the CLDA lies in its simplicity, which allows nonstationary contact-line dynamics problems to be solved in 3D without further linearization or other approximations. When the meniscus motion is slow, the qua-

 ©2008 The American Physical Society

sistatic version of the CLDA [10,11,14] is suitable. When the fluid inertia is essential, e.g., during rapid processes like oscillations of sessile drops [15], the position of the liquid-gas interface needs to be determined from dynamic equations. Since the outer region dissipation is assumed to be negligible with respect to that in the inner region, nonviscous hydrodynamics needs to be applied [12].

The purpose of this paper is twofold. First, we compare the experimental data on highly viscous fluid and the HA results with those of the CLDA in order to check its validity. Second, we analyze the results of the 3D CLD simulation in order to understand the influence of nonlinearity on the relaxation of the contact-line deformation and the limits of applicability of linearized approaches.

II. CLD DESCRIPTION AND PROBLEM FORMULATION

According to the main CLD assumption [13], the energy T dissipated in the system per unit time is the integral over the contact line

$$T = \int \frac{\xi v_n^2}{2} dl, \tag{1}$$

where v_n is the contact-line speed measured in the direction normal to the contact line and ξ is a constant "dissipation coefficient." It has been shown [11,12] that, independently of the interface shape or external forces, the expression (1) leads to the local equation valid at any contact-line point:

$$v_n = \frac{\gamma}{\xi}(\cos\theta_{\mathrm{eq}} - \cos\theta), \tag{2}$$

where γ is the surface tension, θ_{eq} and θ are the equilibrium and local instantaneous (or dynamic) contact angles. Equation (2) is valid independently of whether or not gravity or other external forces are present. The dynamic contact angle is introduced as the angle of the smooth continuation of the outer region meniscus toward the solid surface as in [3]. Since the dynamic contact angle is not a rigorously defined quantity, it is omitted from further consideration and Eq. (1) rather than Eq. (2) is used in what follows.

In general, the CLDA cannot be applied to situations where a thin liquid film forms on the solid. The viscous dissipation in the film is then important and Eq. (1) is not valid. This means that neither the complete wetting nor the high receding velocity at partial wetting where the film is entrained by the plate (as in the dip coating process) can be described by the CLDA. However, it can be applied at small contact-line speeds at partial wetting.

It turns out that the partial wetting regime is the least studied experimentally. The main reason is the strong influence of the inevitable random surface heterogeneity (called surface defects hereafter) on the contact-line dynamics. The presence of surface defects leads to interesting effects like contact-line pinning and depinning transitions [16] but causes poor repeatability of the experiments. Only a few experiments have been described in the literature [3,17–21]. However, the information given in most papers is incomplete and does not permit a direct comparison with the calculation.

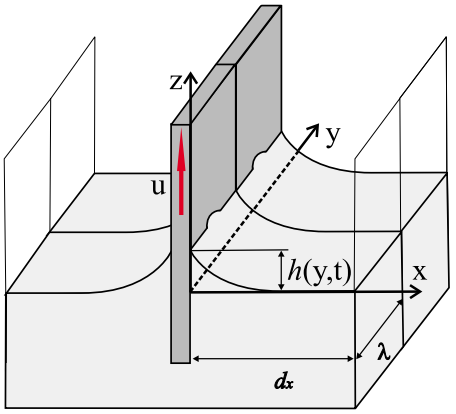

FIG. 1. (Color online) Geometry of the problem.

Only Ref. [3] presents sufficiently detailed information for a comparison to be possible.

As in Ref. [3], the classical "Wilhelmy plate" experiment where a solid plate is withdrawn vertically at constant velocity u from a liquid-filled bath (Fig. 1) is considered here. One of the plate faces (the other is not considered) is described with the Cartesian coordinates (y,z), where the y axis is horizontal and the z axis is directed upward. The liquid meniscus forms a contact line defined by its height $h(y,t)$ where t is the time. We do not consider here the extreme contact-line deformations where such a description is impossible. Since h is measured in the bath reference,

$$v_n = \dot{h} - u, \tag{3}$$

where the dot over h means the time derivative.

The meniscus forms a dynamic contact angle $\theta(y,t)$ with the moving plate. At the vertical bath wall opposite to the moving plate and parallel to it, a right contact angle is assumed. The distance between the plate and the wall is large and is denoted by d_x. The liquid is the same as in [3]: polydimethylsiloxane, a silicone oil with shear viscosity $\eta = 4.95$ Pa s, surface tension $\gamma = 20.3$ mN m^{-1}, and density $\rho = 970$ kg m^{-3}. The capillary length is $l_c = \sqrt{\gamma/\rho g} = 1.46$ mm, where g is the gravity acceleration. The liquid forms the contact angle $\theta_{\mathrm{eq}} = 51.5°$ which corresponds to the static receding contact angle of the experiments [3]. Despite the fact that the contact line always recedes in these experiments, its authors also consider another value of $\theta_{\mathrm{eq}} = 54.3°$, an average of advancing and receding static contact angles. However, when the contact line recedes, the receding static contact angle needs to be used as the microscopic contact angle.

Dimensionless variables will be used in the next section. The plate speed is characterized by the capillary number $\mathrm{Ca} = u\eta/\gamma$. The lengths and times are made dimensionless by using l_c and $\tau = l_c\eta/\gamma$, respectively.

The quasistatic version of the CLDA is appropriate here. This means that the meniscus can be considered as if it were in equilibrium attained for the contact-line position given at each time moment.

III. UNPERTURBED CONTACT LINE

In order to check the validity of the contact-line dissipation model, one needs first to determine its only adjustable

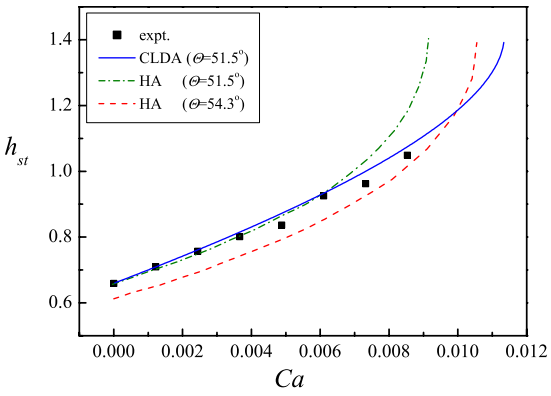

FIG. 2. (Color online) Stationary height of the contact line (expressed in l_c units) as a function of the dimensionless plate speed Ca. The solid squares are the experimental results [3]; the solid line is the solution of Eq. (5) corresponding to ξ=164 Pa s and θ_{eq} =51.5°. The dotted and dashed lines are the HA results [3] for θ_{eq} =51.5° and 54.3°.

parameter, the phenomenological dissipation coefficient ξ. It can be determined from the experimental data [3] on the rise of an unperturbed contact line on a macroscopically homogeneous plate. After a relaxation stage, the contact line attains a stationary height $h_{st}=h(t\to\infty)$ measured [3] as a function of u.

Obviously, $v_n=-u$ here since $\dot{h}_{st}=0$. h_{st} can be calculated from the expression that holds for the equilibrium meniscus [22],

$$h_{st}=\sqrt{2(1-\sin\theta)}. \tag{4}$$

By eliminating θ from the set of equations (2) and (4), one arrives at the relation

$$\mathrm{Ca}=(h_{st}\sqrt{1-h_{st}^2/4}-\cos\theta_{eq})\frac{\eta}{\xi}. \tag{5}$$

By fitting the experimental data [3] with Eq. (5), we find ξ=164 Pa s (Fig. 2). Note that this value is about 30 times larger than the shear viscosity. The ratio ξ/η is much smaller than for low-viscosity fluids, where it can reach enormous values of the order of 10^6-10^7 [8,15]. The relatively small value of this factor shows that the silicone oil case is limiting with regard to the applicability of the contact-line dissipation model. If the latter works for silicone oil, one may expect it to work even better for fluids of lower viscosity.

One can see that the quality of the CLD fit is much better than the HA results (Fig. 2) the best of which corresponds to θ_{eq}=51.5°. The agreement of the HA curve for θ_{eq}=54.3° with the experiment is even worse. However, it is this latter value that was used in [3] for the studies of contact-line dynamics. The former value is used throughout the present work.

Consider now the contact-line rise dynamics where h and θ are both time dependent. By using again (3) and (4), Eq. (2) can be reduced to the following equation:

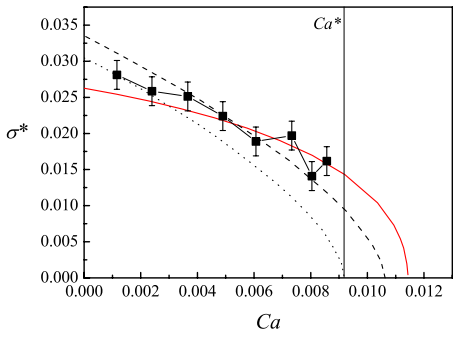

FIG. 3. (Color online) Dimensionless relaxation rate $\sigma^*=\sigma_0\tau$ for the straight contact line as a function of Ca. Experiment [3]: squares with error bars indicating the variation in the experimental results. Results of the exponential fitting of the theoretical solution (7) for $h_0=0.99h_{st}$ and θ_{eq}=51.5° are shown as a solid line. HA results [3] are shown with dotted (θ_{eq}=51.5°) and dashed (θ_{eq}=54.3°) lines.

$$\dot{h}=\mathrm{Ca}+\frac{\eta}{\xi}(\cos\theta_{eq}-h\sqrt{1-h^2/4}). \tag{6}$$

This equation can be solved analytically:

$$\frac{1}{a\sqrt{2}}\left\{-b\left[\frac{1}{\sqrt{1+a}}\mathrm{arth}\left(\frac{h}{\sqrt{2(1+a)}}\right)-\frac{1}{\sqrt{1-a}}\mathrm{arth}\left(\frac{h}{\sqrt{2(1-a)}}\right)\right]-\sqrt{1-a}\,\mathrm{arth}\left(\frac{\sqrt{4-h^2}}{\sqrt{2(1-a)}}\right)+\sqrt{1+a}\,\mathrm{arth}\left(\frac{\sqrt{4-h^2}}{\sqrt{2(1+a)}}\right)\right\}=(t+t_0)\frac{\eta}{\xi}, \tag{7}$$

where arth is the inverse hyperbolic tangent, $a=\sqrt{1-b^2}$, $b=\mathrm{Ca}\,\xi/\eta+\cos\theta_{eq}$ and the constant t_0 is straightforwardly determined from the initial condition $h_0=h(t=0)$. It has been found in [3] that the experimental relaxation of this "zero-mode" perturbation (of infinite period) can be fitted by an exponential function. For this reason, we fitted an exponential function to Eq. (7). The fit is indeed of good quality. However, the relaxation time and its inverse, the relaxation rate σ_0, obtained from the fit turn out to depend slightly on h_0. The latter value could not be measured experimentally [3] and was supposed to be close to h_{st}. The h_0 dependence of the relaxation time is a consequence of the nonlinearity of Eq. (6).

The fit that uses the ξ value found above is compared with the HA results in Fig. 3. The agreement of the CLDA curve with the experiment is significantly better than that for the HA curve with θ_{eq}=51.5° and is of the same quality as that with θ_{eq}=54.3°. However, the HA with θ_{eq}=54.3° does not agree quantitatively with the experimental h_{st}(Ca) dependence shown in Fig. 2. As a matter of fact, Fig. 3 shows the sensitivity of the relaxation time to the value of θ_{eq}. Its 3° change causes a horizontal shift of the whole curve by 10% of its total width.

The stationary meniscus exists when $\mathrm{Ca}<\mathrm{Ca}_c$, a critical value at which θ becomes equal to zero and the meniscus height attains $\sqrt{2}$. For the CLDA, $\mathrm{Ca}_c\simeq 11.4\times 10^{-3}$. How-

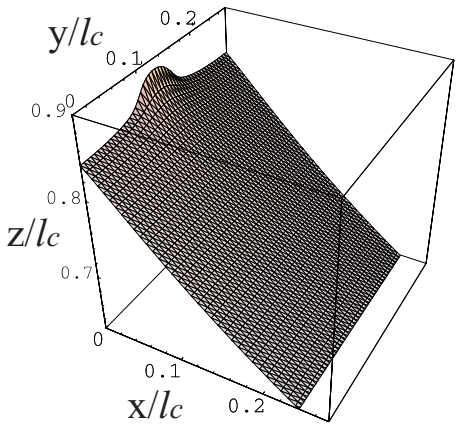

FIG. 4. (Color online) An example of the surface meshing for $\lambda=400$ μm. A part (about 2%) of the initial shape of the meniscus in the vicinity of the contact line is displayed.

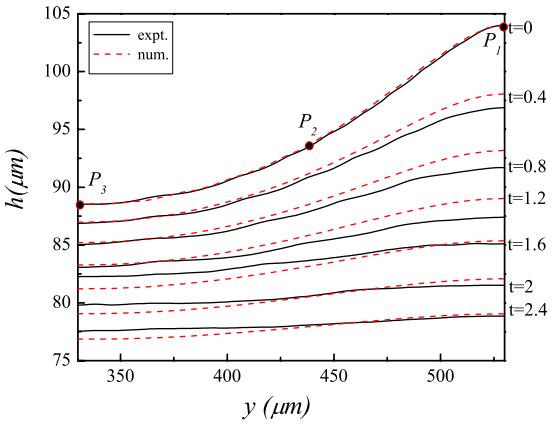

FIG. 5. (Color online) Time evolution of the contact-line profile $h(y,t)$ is shown with time step $\Delta t=0.4$ s at Ca=0.004 76. Only half a period of the initially periodically perturbed contact line with period 400 μm is displayed. Dashed lines, numerical CLDA results; solid lines, experiment [3]. The solid symbols show the positions of three points P_1, P_2, and P_3.

ever, the entrainment of a thin film by the plate has been observed in the experiment at $\mathrm{Ca}=\mathrm{Ca}^*=9.1\times10^{-3}<\mathrm{Ca}_c$, which corresponds to the Landau-Levich transition. As mentioned above, the CLDA cannot describe this case.

We also find that within the CLDA the relaxation rate scales with Ca as $\sigma^*\sim(\mathrm{Ca}_c-\mathrm{Ca})^{0.4}$. This exponent is close to the predictions of the linearized quasistatic theory of Golestanian and Raphaël [23] and of the linearized HA [2] both of which lead to the exponent 0.5.

IV. MOTION OF A PERIODICALLY DEFORMED CONTACT LINE

In the experiment [3], the contact line was deformed after having passed through a horizontal row of periodic defects spaced at $\lambda=400$ or 600 μm for the same liquid-substrate combination and for the same range of Ca as in the previous section. Therefore we can use for the dissipation coefficient the value $\xi=164$ Pa s determined above.

We study the relaxation dynamics of a periodically deformed contact lines (which is a genuine 3D problem) by adapting the numerical code developed earlier for the sessile droplet geometry [11].

A. Description of the numerical algorithm

The main ingredients of this algorithm are the determination of the liquid interface (meniscus) shape with given volume of the liquid and given contact line, and the calculation of the velocity of the contact line.

The meniscus shape is determined by an iterative minimization procedure based on the local variations method [24]. We give here only a concise description; more details can be found in [25]. The meniscus is approximated by a set of triangles with vertex points $R[x_i,y_j,z(x_i,y_j)]$ called nodes; $i=1,\ldots,N_i$; $j=1,\ldots,N_j$ (see Fig. 4). The numerical results reported below are obtained with $N_j=51$, $N_i=600$, and $d_x=17.3l_c$. The surface of the meniscus is determined in terms of the coordinates of $N_i\times N_j$ nodes. The randomly chosen displacements of $(N_i-1)\times N_j$ nodes are considered under the constraint of keeping unchanged the volume and the first N_j nodes that belong to the contact line. Only those displacements that reduce the free energy of the system are retained.

The surface dynamics is simulated as follows. First, for a given position of the contact line the stationary shape of the meniscus of the liquid with fixed volume V in the domain enclosed between the planes $y=0$ and $y=\lambda$ is determined as described above. The periodic boundary conditions in the y direction are imposed (see Fig. 1). Next, v_n at every contact-line node is obtained directly from the equality of the variations of the free energy and of the contact-line dissipation (see [11] for more details). This method is preferred over the direct application of Eq. (2) because it does not require θ calculation. Using the latter would lead to an important accuracy loss when the contact line is curved. The contact-line position at the next time step is found explicitly by using v_n. This algorithm is repeated for the successive time steps.

B. Numerical simulation of the relaxation of a periodically perturbed contact line

In Fig. 5 of Ref. [3] the profiles of the relaxing contact line are shown with time step $\Delta t=0.4$ s for an initially periodically perturbed contact line with a period $\lambda=400$ μm and for plate speed Ca=0.004 76. Such detailed information (which was absent from other papers [17–21] on the controlled contact-line deformation) allows the CLDA to be tested against the experiment.

For convenience the contact-line profiles are reproduced here (solid lines) in Fig. 5 where only a half period of the contact line from Fig. 5 of Ref. [3] is shown. We treat only a half period because of the periodic geometry under consideration. In the experiment, both asymmetry and nonperiodicity occur inevitably because of the contact-line pinning on the residual random surface defects. The time decay of the long-range spatial correlation of the contact line position becomes even more obvious when the evolution of the whole extension (four periods) of the contact line is displayed [26].

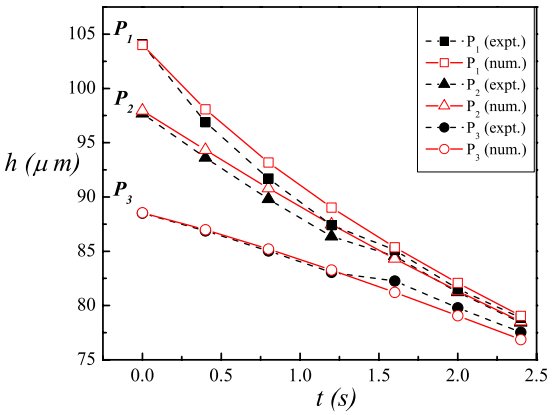

FIG. 6. (Color online) Time variation of the heights of the points P_1, P_2, and P_3 indicated with solid symbols in Fig. 5. Solid lines and solid symbols, experimental results [3] (P_1, squares; P_2, triangles; P_3, circles). Open symbols and dashed lines, numerical CLDA results.

The initial contact-line shape for the simulation has been defined with the experimental contact line at $t=0$ (see Fig. 5). However, it is not exactly symmetric. We therefore generate a periodic contact line which coincides at the half period ($y \in [330,530]$ μm) with the experimental contact line. The numerical solutions obtained for the contact-line profiles at the same time step are shown in Fig. 5 with dashed lines.

In order to estimate the quality of the experimental data approximation, the time relaxation of three selected points P_1, P_2, and P_3 (see Fig. 5) defined by their y values is compared with the experiment (Fig. 6). P_1 ($y=530$ μm) is the maximum of the contact line, P_3 ($y=330$ μm) is the minimum of the perturbed line, and P_2 ($y=474$ μm) is an intermediate point. The time variations of P_1 and P_2 are fitted successfully by exponential decay functions; the time variation of the inverse height of the point P_3 can be fitted by an exponential decay function. The CLDA and experimental relaxation times agree within 2–4 %. The same holds if one compares the numerical results obtained as described above to the experimental results in the interval $y \in [0,800]$ μm (not shown in Fig. 6).

C. Relaxation rates and nonlinearity

We now address the problem of the dependence of the relaxation rates on the wave number q ($q=2\pi/\lambda$) of the perturbation of the contact line. The quasistatic approach [23] results in the relaxation rate σ (the inverse of the relaxation time) proportional to q

$$\sigma(q) = |q| f(\mathrm{Ca}) \tag{8}$$

under the assumptions that (i) $\lambda \ll l_c$ and (ii) the meniscus slope is small ($|\nabla h| \ll 1$). This result has been obtained previously for Ca=0 within the linear "contact-line elasticity" theory [27]. The same result has been recovered for arbitrary Ca in the framework of the linearized HA [2]. We would like to underline that in all these cases the small-slope approximation has been used explicitly or implicitly.

Here we study the relaxation rates for relatively large meniscus slopes. One can proceed as suggested in [3] and fit the profiles of the contact lines with a three-mode Fourier decomposition,

$$h(y,t) = a_0(t) + a_1(t)\cos(qy + y_0) + a_2(t)\cos(2qy + y_0) + a_3(t)\cos(3qy + y_0), \tag{9}$$

where $a_0(t)$, $a_1(t)$, $a_2(t)$, and $a_3(t)$ are the time-dependent amplitudes.

First we analyze the relaxation rates at Ca=0.004 76 of the numerical and experimental contact lines shown in Fig. 5. The amplitudes $a_i(t)$, $i=1,2,3$, are fitted successfully with the exponential decay functions $a_i(t)=A_i \exp(-t/\tau_i)$ where τ_i are the relaxation times. The values for the relaxation times τ_i^n of the numerical data are 1.28, 0.73, and 0.52 s for $i=1,2,3$, respectively. The fitting function of the amplitude $a_0(t)$ is similar to that of the height of the point P_3. Since the experimental contact lines (Fig. 5) are not exactly periodic, the relaxation times τ_i^e depend on the interval where the Fourier decomposition is performed. For the Fourier decomposition of the experimental contact lines only on $\lambda/2$ (interval $[330,530]$ μm) to enforce the periodicity, one obtains the relaxation times 1.1, 0.78, and 0.48. The coefficients of the Fourier decomposition of the numerical, $a_i^n(t)$, and of the experimental data, $a_i^e(t)$, agree within 10%. Thus the Fourier analysis confirms that the CLDA is suitable to describe the experimental data.

One can see, however, that the relaxation times obtained in the time interval $t \in [0,2.4]$ s do not follow the proportionality pattern $1:1/2:1/3$, in disagreement with Eq. (8). The violation of the above pattern appearing in both the numerical and experimental results can be attributed only to the importance of the meniscus slope, i.e., of the nonlinearity. The latter is characterized mainly by $|\partial h/\partial y|$ which attains 0.12 at $t=0$. Apparently this value is sufficiently large for the appearance of nonlinear effects.

The analysis of the simulated relaxation shows that the relaxation times obtained at the late stages of the relaxation (where the slope is smaller) resemble more closely the linear theory. Indeed, for $t \in [3.6,5.6]$ s, the exponential fitting yields the (numerical) relaxation times $\tau_i^n=1.21$, 0.64, 0.403 s for $i=1,2,3$ respectively. They result in the proportionality pattern 1:0.53:0.33 which is much closer to $1:1/2:1/3$ than that of the early stage. Generally speaking, the variation of the relaxation time with the interval of fitting means that the relaxation curve is not exponential. This shows once again the significance of the nonlinearity in the system.

In [3] the fitting of the contact-line profiles by Eq. (9) has been performed for $t \in [0,2.4]$ s on the interval 2λ instead of 0.5λ here. They obtained the relaxation times $\tau_i^e=1.07$, 0.49, and 0.4 s for $i=1,2,3$, respectively. Note that the relaxation times change noticeably. We attribute this discrepancy to the influence of the "background" random surface defects that lead to long-range spatial correlation of the contact-line position that decreases with time and thus to loss of periodicity.

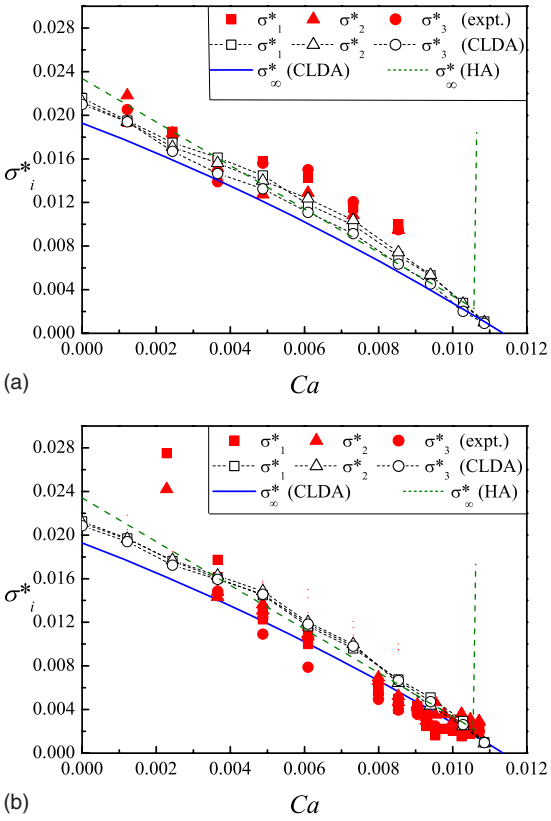

FIG. 7. (Color online) Dimensionless relaxation rates σ_i^*, $i=1,2,3$, as functions of the capillary number Ca. Solid symbols, experimental data fitting results from Fig. 7(b) of [3]. Open characters, CLDA ($\theta_b=\theta_{eq}-1°$, $\theta_{eq}=51.5°$). The squares, triangles, and circles correspond to σ_1^*, σ_2^*, and σ_3^*, respectively. $\lambda=$(a) 400 and (b) 600 μm. The solid line is a result of the linearized CLDA for $\sigma_\infty^{*\mathrm{CLD}}$ and the dashed line is the HA result [3] for $\theta_{eq}=54.3°$.

D. Dependence of the relaxation rates on Ca

In what follows we consider the dependence of the relaxation rates on Ca and on the period λ of the deformation of the contact line. The dimensionless relaxation rates are defined as $\sigma_i^*=\eta\lambda/(2\pi i\tau_i)$, where τ_i is the corresponding relaxation time for the mode $i\in(1,2,3)$.

It was shown in the previous section that the nonlinearity related to the meniscus slope can be considered negligible only at the very end of the relaxation where h is small. Therefore it would be desirable to control the initial interface shape. For this purpose, we choose for the initial condition the stationary position of the contact line on a plate with periodic (period λ) vertical bands of width 0.2λ. The wetting properties of the bands are chosen to be different from those of the rest of the plate. The stationary contact angle θ_b at these bands is assumed to be smaller than the contact angle at the rest of the plate equal to θ_{eq}. At $t=0$ the value of θ_b is changed instantaneously to θ_{eq} and the relaxation begins.

Consider first a small initial contact-line perturbation corresponding to $\theta_b=\theta_{eq}-1°$. The corresponding relaxation rates are plotted in Figs. 7(a) and 7(b) as functions of Ca for perturbations of wavelengths $\lambda=400$ and 600 μm, respectively. The numerical data are obtained for the whole interval

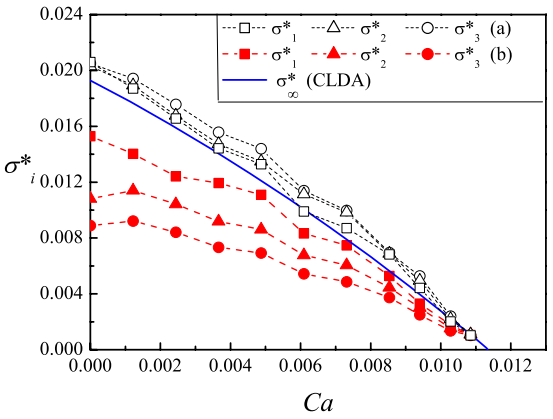

FIG. 8. (Color online) Dimensionless relaxation rates σ_i^*, $i=1,2,3$, as functions of the capillary number Ca for strong initial perturbations for $\lambda=400$ μm and $\theta_{eq}=51.5°$. Symbols and dashed lines, the CLDA numerical results. Open symbols, case (a) where $\theta_b=\theta_{eq}-4°$; solid symbols, case (b) where $\theta_b=5°$. The solid line for $\sigma_\infty^{*\mathrm{CLD}}$ is shown to enable the comparison with Fig. 7. The squares, triangles, and circles correspond to σ_1^*, σ_2^*, and σ_3^*, respectively

of plate speeds $0\leqslant \mathrm{Ca}<\mathrm{Ca}_c$. The experimental data [3] (obtained when the fitting of the contact-line profiles is performed over the interval 2λ) are reproduced here with the solid symbols.

Since the period of the considered perturbations is such that $\lambda\ll l_c$, we can compare our results with the relaxation of a contact line in the limit of large wave numbers $q\to\infty$. The linearized quasistatic approach [2] (equivalent to the linearized CLDA) leads to the following relation:

$$\sigma_\infty^*=\sigma^* g(\theta_{eq}),\quad g(\theta_{eq})=\frac{|\cos\theta_{eq}|\sin\theta_{eq}}{h_{st}},\qquad (10)$$

where σ_∞^* is made dimensionless similarly to σ_i^*. One can test this relation to estimate $\sigma_\infty^{*\mathrm{CLD}}(\mathrm{Ca})$ from the CLDA curve for the unperturbed contact line shown in Fig. 3. This result is displayed in Figs. 7 and Fig. 8 with the solid lines. The HA prediction calculated [3] for the median value $\theta_{eq}=54.3°$ is also reproduced.

According to Fig. 7, the CLDA and experimental results for the relaxation rates as functions of Ca appear to be in good agreement. However, the $\sigma_\infty^{*\mathrm{CLD}}(\mathrm{Ca})$ curve deviates from the numerical CLDA curve. This discrepancy is another manifestation of the nonlinearity: the expression (10) was obtained due to linearization. The results of the CLDA are as close to the experiment as the HA results. We recall, however, that the latter results were obtained for another value of the contact angle. The CLDA relaxation rates scale with Ca as $\sigma^*\sim(\mathrm{Ca}_c\text{-}\mathrm{Ca})^\beta$, $\beta\in[0.65,0.85]$. The results of the linearized HA lead to the exponent 1.

To reveal the influence of the nonlinearity on the relaxation, it is interesting to simulate stronger initial perturbations of the contact line than those considered up to now. In Fig. 8 we present the CLDA relaxation rates for $\theta_b=\theta_{eq}-4°$ and for $\theta_b=5°$. The latter choice approaches the maximal amplitude of the perturbation where the surface can still be described by the single-valued function $z=h(x,y)$ and

where $|\nabla h| \gg 1$. For the sake of comparison we mention that the initial contact line ($t=0$) in Fig. 5 can be well approximated by the stationary contact line on a striped surface considered in this section where $\theta_b = \theta_{eq} - 10°$ at the band, and the contact angle equal to $\theta_{eq} - 6°$ at the rest of the plate.

The relaxation rates depend also on the width of the band. For example, if the width of the band is increased twice, the relaxation times increase by about 15%.

One can see that an increase of the contact-line perturbation causes a decrease of the relaxation rates. This is the effect of the nonlinearity, analogously to that discussed for the unperturbed contact line. Indeed, Fig. 8 shows that the dependence $\sigma(q)$ becomes weaker than linear [i.e., it seems that $\sigma(q) \sim q^{\kappa}$, where $\kappa < 1$]. The same tendency can be traced in the experimental data of Fig. 7(b) (the solid circles are below the squares and the triangles) although no definitive conclusion is possible because of the experimental data scatter. We find also that at large deformations the scaling changes: the relaxation rates scale with Ca as $\sigma_i^* \sim (\mathrm{Ca}_c - \mathrm{Ca})^{\beta}$, $\beta \in [0.3, 0.4]$.

V. CONCLUSIONS

This work deals with numerical simulations of the general nonlinear 3D problem within the contact-line dissipation approach. To the best of our knowledge, only linear (or linearized) analysis of the dynamics of contact-line relaxation was available up to now.

A detailed comparison with the experimental data of Delon *et al.* [3] and with their hydrodynamic approach has been performed. In the framework of the hydrodynamic approach initially applied [2,3] to interpret their experimental data, two different values of contact angle were needed to describe different experimental data sets. The CLDA parameters allowed a good agreement to be achieved using the single, actually measured value of the contact angle. Note that the relaxation times are very sensitive to the contact angle value. As a matter of fact, this sensitivity explains experimental data scatter appearing because of the solid surface heterogeneity (which can be interpreted as a random variation of the local contact angle).

An advantage of the CLDA with respect to other approaches is its simplicity. The CLDA involves a single adjustable parameter (the constant dissipation coefficient ξ), which has been determined from the experimental data on stationary meniscus height as a function of Ca and then was used to describe the dynamic experiments.

The CLDA has been validated here against experimental data for a limiting case with regard to its applicability: a strongly viscous fluid. It is expected to work even better for low-viscosity fluids (where the HA is more difficult to apply).

A study of the influence of the surface nonlinearity on the contact-line relaxation has been carried out. It has been shown that the contact-line elasticity theory derived initially in the linear approximation (small interface slopes) fails at even moderate slopes. An increasingly large surface slope leads to a decrease of the relaxation rate σ and to an increase of the deviation of the $\sigma(q)$ curve (q is the wave number) from the linear dependence predicted within the contact-line elasticity theory. The simulations predict that the $\sigma(q)$ dependence should become weaker than linear with increasing amplitude of the meniscus deformation.

To summarize, the CLDA presents a powerful tool that can be applied to future studies, e.g., of the collective effect of surface defects on contact-line motion (dynamic hysteresis, etc.).

ACKNOWLEDGMENTS

We thank the authors of [3] for giving us the experimental data prior to its publication. S.I. has received financial support from the NSF-Bulgaria under Grant No. VU-MI-102/05. S.I. is grateful to the laboratory of Physics and Mechanics of Heterogeneous Media of ESPCI for its kind hospitality.

[1] R. Golestanian and E. Raphaël, Phys. Rev. E **67**, 031603 (2003).
[2] J. Snoeijer, B. Andreotti, G. Delon, and M. Fermigier, J. Fluid Mech. **579**, 63 (2007).
[3] G. Delon, M. Fermigier, J. Snoeijer, and B. Andreotti, J. Fluid Mech. **604**, 55 (2008).
[4] J. F. Joanny and M. O. Robbins, J. Chem. Phys. **92**, 3206 (1990).
[5] V. S. Nikolayev (unpublished).
[6] W. Boender, A. K. Chesters, and A. J. J. van der Zanden, Int. J. Multiphase Flow **17**, 661 (1991).
[7] J. H. Snoeijer, Phys. Fluids **18**, 021701 (2006).
[8] C. Andrieu, D. A. Beysens, V. S. Nikolayev, and Y. Pomeau, J. Fluid Mech. **453**, 427 (2002).
[9] J. Eggers and H. A. Stone, J. Fluid Mech. **505**, 309 (2004).
[10] V. S. Nikolayev and D. A. Beysens, Europhys. Lett. **64**, 763 (2003).
[11] S. Iliev, N. Pesheva, and V. S. Nikolayev, Phys. Rev. E **72**, 011606 (2005).
[12] V. S. Nikolayev, S. L. Gavrilyuk, and H. Gouin, J. Colloid Interface Sci. **302**, 605 (2006).
[13] M. J. de Ruijter, J. de Coninck, and G. Oshanin, Langmuir **15**, 2209 (1999).
[14] V. S. Nikolayev, J. Phys.: Condens. Matter **17**, 2111 (2005).
[15] R. Narhe, D. Beysens, and V. Nikolayev, Langmuir **20**, 1213 (2004).
[16] S. Moulinet, C. Guthmann, and E. Rolley, Eur. Phys. J. B **37**, 127 (2004).
[17] A. Paterson, M. Fermigier, P. Jenffer, and L. Limat, Phys. Rev. E **51**, 1291 (1995).
[18] J. A. Marsh and A.-M. Cazabat, Phys. Rev. Lett. **71**, 2433 (1993).
[19] G. D. Nadkarni and S. Garoff, Europhys. Lett. **20**, 523 (1992).
[20] T. Ondarçuhu and M. Veyssié, Nature (London) **352**, 418

(1991).
[21] T. Ondarçuhu, Mod. Phys. Lett. B **6**, 901 (1992).
[22] L. D. Landau and E. M. Lifshitz, *Fluid Mechanics* (Pergamon Press, Oxford, 1987).
[23] R. Golestanian and E. Raphaël, Phys. Rev. E **64**, 031601 (2001).
[24] F. L. Chernousko, Comput. Math. Math. Phys. **4**, 749 (1965).
[25] S. Iliev, Comput. Methods Appl. Mech. Eng. **126**, 251 (1995).
[26] G. Delon, Ph.D. thesis, University Paris 7 Paris, 2007.
[27] P.-G. de Gennes, Rev. Mod. Phys. **57**, 827 (1985).